Al-in-Hornblende Barometry of Southern New England Intrusions and Comparison with Metamorphic Bathograds

Theodore Kuhn

Adviser: Jay Ague, Geology and Geophysics

Second Reader: David Evans, Geology and Geophysics

A Senior Thesis presented to the faculty of the Department of Geology and Geophysics, Yale University, in partial fulfillment of the Bachelor's Degree.

Abstract

The depth of exposure—the original depth at which surficial igneous rocks crystallized or the maximum depth to which surficial metamorphic rocks were buried—is an important factor for understanding the history and processes of orogenic belts. Few quantitative estimates of plutonic emplacement depth in southern New England have been published, and while attempts to map maximum metamorphic pressures such as those of Carmichael (1978) provide a broad regional framework, they rely on reactions with poorly constrained thermodynamic properties and are based on few data points. In this study, the aluminum-in hornblende barometer and pseudosection analysis were used to bring quantitative clarity to the picture of southern New England's baric regime. Pseudosections were generated using a range of compositions and multiple versions of thermodynamic databases to assess metamorphic mineral assemblages useful for P-T estimation. The stability of staurolite showed marked differences between pseudosections using different databases, calling into question the utility and reliability of the staurolite-based bathograds (metamorphic isograds of constant pressure) in Carmichael (1978) and Pattison (2001). An adjusted set of bathograds is proposed that includes new bathograds utilizing the intersections of mineral reactions with the solidus. The aluminum-in-hornblende barometer was used to estimate emplacement pressures for plutonic rocks from eight formations in Connecticut and Rhode Island, providing the first such estimates for igneous rocks in the region. The lowest emplacement pressures (~0.35 GPa ± 0.06 GPa) are found in the Taconic accretionary prism immediately east of Cameron's Line. Higher pressures of ~0.7 GPa are located in the northern Bronson Hill Anticlinorium and the Central Maine terrane, while Avalonian rocks of the Hope Valley Belt and Scituate Igneous Suite were predominantly emplaced at 0.5-0.6 GPa.

1. Introduction

Quantifying the pressure at which plutons crystallized is vital for the development of models of orogenic histories, as dated plutons of known emplacement depth provide fixed "nails" in time and space that can constrain the path of material through the crust (Anderson et al. 2008). Buddington noted in 1959 that "It is rare that estimates are given in the literature of the depths at which the present exposed parts of a pluton were intruded." While thermobarometry has produced numerous pressure estimates for exposed plutons in other parts of the world, Buddington's observation still holds true for southern New England, as quantitative pressure estimates for the region's igneous rocks are nearly non-existent in the literature.

Prior attempts to characterize the depth of exposure of southern New England's igneous rocks have inferred depth based on the metamorphic grade of the surrounding rock, structural characteristics of the intrusion and country rock, and deformational characteristics within the intrusion such as foliation. Buddington used this method to classify plutons into three overlapping depth zones—epizonal, mesozonal, and catazonal, corresponding to approximate pressures of <0.25 GPa, 0.2 GPa-0.45 GPa, and >0.25 GPa. Plutons in Connecticut and Rhode Island are classified by Buddington as epizonal (Cowesett granite, Narragansett Pier granite batholith, Westerly granites), mesozonal (Scituate Granite Gneiss, Prospect Gneiss, Nonewaug Granite), and catazonal (Killingworth dome, Stony Creek Granite and Clinton domes).

A number of limitations exist for these estimates. Pressure estimates derived from metamorphic rock during the time of Buddington have since been adjusted significantly. Though modern thermobarometric methods produce more accurate metamorphic pressure estimates, this

method is only useful when wall rocks and roof pendants with suitable mineral assemblages for pressure estimation are present and unequivocally at the same structural level, which is relatively rare (Ague 1997). Overprinting of the surrounding rock post-emplacement is also common (Zen, 1989). Al-in-hornblende (AH) barometry provides a solution to these problems in that it does not rely on the character of the surrounding rocks to estimate the depth of crystallization. This paper uses the AH barometer to quantitatively estimate the depth of crystallization of a number of plutonic rocks from Connecticut and Rhode Island.

Metamorphic pressures are similarly vital in understanding orogenic processes. A semi-quantitative description of the maximum metamorphic pressure regime in New England was first proposed by Carmichael (1978). This scheme divides the region's surface into a series of bathozones, areas of approximately equal maximum pressure that are bracketed by bathograds, metamorphic isograds that vary with pressure but are ideally independent of temperature (Thompson and Norton, 1968). These bathograds are based on the locations of invariant points in a ten-mineral model system typical of New England (Figure 7). The mineral assemblages of the higher and lower-pressure fields on either side of the invariant point can be used to identify which bathozone and associated pressure range a rock belongs to without the need for a more involved modal or compositional analysis.

Carmichael's bathozones indicate a southward and westward increase in pressure for New England, with pressures lowest in Maine and highest in southwestern Connecticut (Figure 1), which Carmichael notes is in broad agreement with qualitative indicators of metamorphic depth; Connecticut's geology is largely characterized by high-grade gneisses and schists with migmatitic features common, suggesting that its surface exposes the lower "roots" of the

orogenic belt, while in northern New England distinct contact aureoles and lower metamorphic grade suggest a shallower depth of exposure.

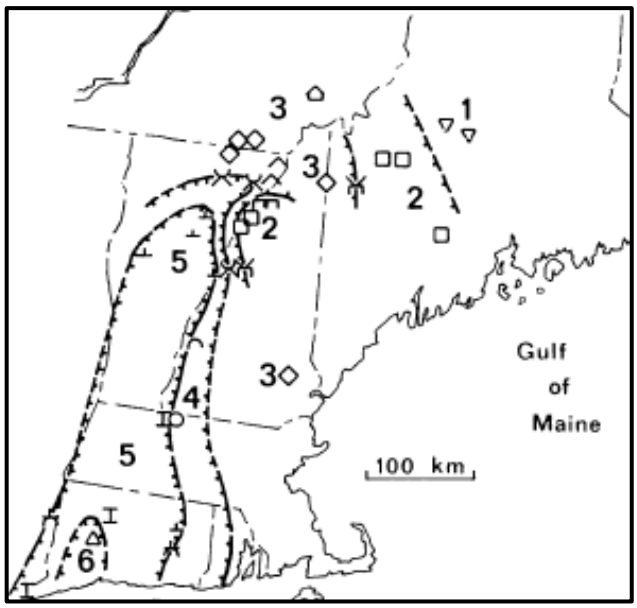

Figure 1. The bathozones of Carmichael (1978). The point symbols indicate the locations of mineral assemblage observations upon which the locations of the bathograds were based. See Figure 7 for the pressure bounds and mineralogical basis of each bathozone.

Though Carmichael's bathograds provide a useful initial framework by which to understand broad regional trends in depth of exposure, few sampling points constrain the bathograds in southern New England (six in Connecticut, zero in Rhode Island). More recent pressure estimates using a variety of methods suggest a more spatially variable and generally deeper pattern than that of Carmichael (Figure 2). Thermobarometric estimates broadly corroborate Carmichael's bathozones; two estimates from Carmichael'bathozone 5, which is meant to reflect pressures of ~0.5-0.7 GPa, have values of 0.6 GPa (Dipple et al. 1990) (Hames et al. 1991), while two from bathozone 6 (>0.7 GPa) have values of 0.82 and 1.0 GPa (Hames et al. 1989) (Dietsch 1989). Other methods show substantial deviations from the bathozone estimates. Pseudosection analysis at two localities in bathozone 5 give lithostatic pressures of 0.8 and 1.8 GPa (Chu et al. 2016) (Keller 2016). Wintsch et al. (2003) modeled pressure-

temperature-time paths for four locations in the Bronson Hill Arc (bathozone 5), using thermochronological constraints and a crustal model to estimate maximum pressures

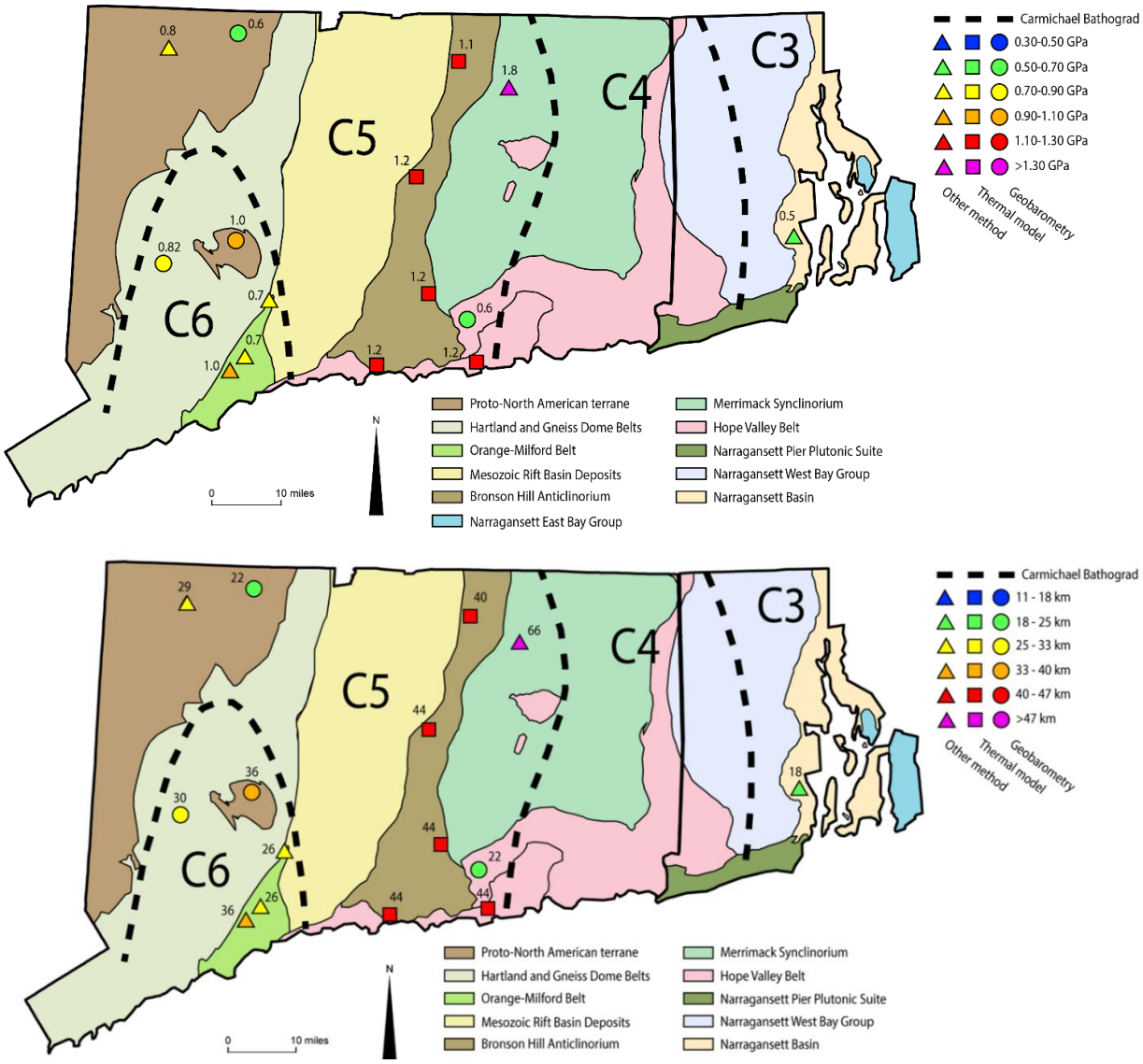

Figure 2. Metamorphic pressure (top) and depth (bottom) estimates from the literature. All pressures are in GPa. Depths are in km and are calculated assuming pressures are entirely lithostatic and a crustal density of 2800 kg m^{-3}. Bathograds traced from Carmichael (1978). Pressure estimates are from the following studies by region: Proto-North American terrane: Chu et al. (2016), Hames et al. (1991), and Dietsch (1989). Orange-Milford Belt: Ague (2002). Bronson Hill Anticlinorium: Wintsch (2003). Merrimack Synclinorium: Keller and Ague (2016). Hope Valley Belt: Walsh et al. (2007) and Dipple et al. (1990). Narragansett Basin: Grew and Day (1972). Geologic map based on "Generalized Bedrock Geologic Map of Connecticut", CT DEEP, 2013.

of ~1.2 GPa, and Walsh et al. (2007) used similar methods to estimate pressures of ~1.2 GPa in the Lyme Dome (bathozone 5).

Attempts have been made to update the bathograd scheme of Carmichael (1978), notably by Pattison (2001). Thermodynamic data for key pressure-constraining minerals have since been updated, suggesting the need for a reassessment of these bathograd schemes. To that end, pseudosections utilizing two generations of thermodynamic data and a wide range of compositions are examined in this study.

2. Methods

2.1 The Aluminum-in-Hornblende Barometer

The utility of the AH barometer is grounded in the observation by Hammarstrom and Zen (1986) that the total aluminum content of hornblende that has equilibrated in rocks containing quartz, plagioclase, K-feldspar, biotite, titanite, Fe-Ti oxides, supercritical fluid, and melt increases with pressure. Ague (1997) proposed the following tschermak-type exchange reaction as one potential barometric reaction governing the Al-content in granitic hornblende:

tremolite + phlogopite + 2anorthite + 2albite = 2pargasite + 6quartz + K-feldspar (1)

This reaction, based on the thermodynamic data and activity models of Mäder and Berman (1992) and Mäder et al. (1994) for amphibole end members, provides a thermodynamic basis for the observed trend of increasing aluminum with pressure, as tremolite is the low-P amphibole end member in the reaction and is devoid of aluminum while pargasite is the high-P end member and contains significant aluminum. This reaction has the benefits of not requiring a-priori

assumptions of a_{H2O}, magma composition, or T, nor the presence of titanite, Fe-Ti oxides, or melt, broadening the range of compositions for which the barometer can be used. Pressure estimates based on Ague's reaction closely mirror those produced by experimental calibrations of aluminum in hornblende such as that of Schmidt et al. (1992), suggesting that the additional compositional constraints and assumptions of Hammarstrom and Zen (titanite, Fe-Ti oxides, melt, etc.) are not required to estimate pressure using an experimental relationship such as that of Schmidt et al. Absolute pressure estimates still vary depending on the calibration used because of the temperature sensitivity of Al in hornblende and the different experimental conditions used; this will be discussed below. Estimates from the AH barometer typically record the pressure at the time of crystallization, as Al diffuses extremely slowly through hornblende below temperatures of ~650°C (Hammarstrom and Zen, 1986). Until the diffusion behavior of aluminum in hornblende under different conditions is extensively studied, the textural appearance and zonation of the crystal must be relied upon to judge the alteration history, or lack thereof, of hornblendes used for barometry.

2.2 Hornblende Compositional Analysis

Thin sections of plutonic rocks containing hornblende were analyzed using the JEOL-JXA 8530F field emission gun electron probe microanalyzer (FEG-EPMA) at Yale University. Between six and ten point analyses from different hornblende crystals in textural equilibrium with their surroundings were carried out for each thin section, including both rim and interior positions. All thin sections were inspected by backscattered electron (BSE) microscopy to detect variations in hornblende composition. This is based on the observation that variations in hornblende composition due to zonation and alteration cause variable BSE brightness (Ague 1996). In thin sections where hornblendes exhibited discernable compositional variability,

separate sets of analyses were carried out for those locations with dark and light BSE brightness respectively to characterize the chemical zonation.

3. Barometry Results

Hornblende analyses are presented in Tables 4 and 5 in the appendix. AH pressures were calculated using the calibrations of Schmidt et al. (1992), Mutch et al. (2016) and Ague (1997). These are presented in Table 1 along with information about the units from which the samples were taken.

Hornblendes were observed to be primarily homogeneous within-sample in aluminum content, as inferred by BSE brightness and confirmed by the microprobe measurements. In those classified as homogeneous, the variation in Al_{tot} between spot analyses did not exceed ~8%. For a representative sample for which the Al_{tot} averaged over all spot analyses gives a pressure of 0.61 GPa by the calibration of Schmidt, this corresponds to a variation of ± 0.07 GPa. This is in line with the uncertainty assigned by Schmidt to their calibration of 0.06 GPa, and with the uncertainty in the calibration of Mutch et al. (2016). This uncertainty arises from the fact that aluminum concentration in hornblende varies naturally and independently of pressure within a single sample of granite, with a typical standard deviation of 0.12 apfu (aluminum per formula unit) for the hornblendes within a sample (Hollister et al. 1987); hence a calibration slope of ~0.5 GPa / apfu yields an uncertainty of 0.06 GPa.

4. Discussion of Barometry Results

The pressures calculated by the calibrations of Mutch et al. (2016), Ague (1997) and Schmidt et al. (1992) differ systematically due to differences in their calibrations (Table 1). The average pressure of hornblendes in this study calculated by the equation from each study is 0.48, 0.53 and 0.59 GPa respectively. The differing estimates can be largely related to the temperature of crystallization used by each calibration. Aluminum content in hornblende increases with increasing crystallization temperature, so a hornblende that crystallized at a temperature lower than that used by the calibration will have a lower aluminum content than that expected by the calibration for a crystal formed at that pressure; as a result, the calibration will underestimate the pressure of crystallization (Ague 1997). The calibrations of Mutch et al. (2016) and Ague (1997) used samples with average equilibration temperatures of 725°C, while the temperatures in Schmidt's calibration ranged from 655°C at 0.95 GPa to 700°C at 0.25 GPa. The lower temperature of Schmidt's calibration explains why it consistently produces the highest pressure estimates in these results. The temperatures of Schmidt are likely an underestimate of actual hornblende equilibration temperature, and hence its pressure estimates are likely an overestimate. The calibration curve of Mutch et al. (2016) lies below the bulk of the experimental and natural data, producing what is likely an underestimate. A map of the calculated pressures based on the calibration of Ague (1997) are displayed in Figure 3, and for the rest of this paper the pressures used will be those of the Ague (1997) calibration unless otherwise noted. The equation from Ague (1997) used to estimate pressure is below:

$$P\ (\pm 0.6\ GPa) = 0.295 \times (Al_{tot}^{1.136}) - 0.07747 \quad (2)$$

No pressure was calculated for sample NE103 as its amphiboles were calcic and therefore not suitable for AH barometry (Mäder et al. 1994). Hornblendes from samples NE11 and NE131 in the Brookfield plutonic series showed zonation with significantly different pressures estimates

from light and dark BSE areas. Chemical maps created for sample NE11 reveal three separate classes of aluminum concentration within the samples' hornblende crystals. The highest-aluminum areas are in the vicinity of grain boundaries with biotite and feldspar. Their location at the edges of the crystal and proximity to biotite, a mineral through which aluminum diffuses relatively rapidly, suggests that these are the effects of later alteration, perhaps during burial after crystallization (as would be supported by the higher aluminum content and pressure estimate of 0.54 GPa). The darker analyses, which produced pressures of ~0.34 GPa and comprised the largest and most interior portions of the hornblendes, are interpreted to represent the initial composition at the time of crystallization. A third zone within the crystals surrounded cracks and appeared very dark in BSE. These were not analyzed for composition but are interpreted to be zones of aluminum-loss that developed due to alteration at lower pressure. The pressure of the most aluminous zones of NE11 is very similar to that of NE10 (0.54 GPa), a sample with homogeneous hornblendes from nearby in the same unit (the Brookfield plutonic series). Counter to the interpretations based on appearance in BSE, this suggests that the most aluminous portions of NE11 are in fact primary, and that the majority of the hornblendes' area has been altered. More detailed analysis of the chemical maps of NE11 will be required to resolve this discrepancy.

Pressure estimates for Connecticut and Rhode Island (Figure 3) exhibit variability that is greater than the error in measurement (± 0.06 GPa), as crystallization pressures range from 0.34 GPa to 0.74 GPa. However, ten out of the fifteen pressures interpreted to be primary crystallization pressures fall between 0.50 GPa and 0.61 GPa, within a range of only 0.11 GPa. Assuming an average crustal density of 2800 kg m^{-3} and that these pressures are lithostatic, this most-common range corresponds to crustal depths of approximately 18-22 km. For comparison,

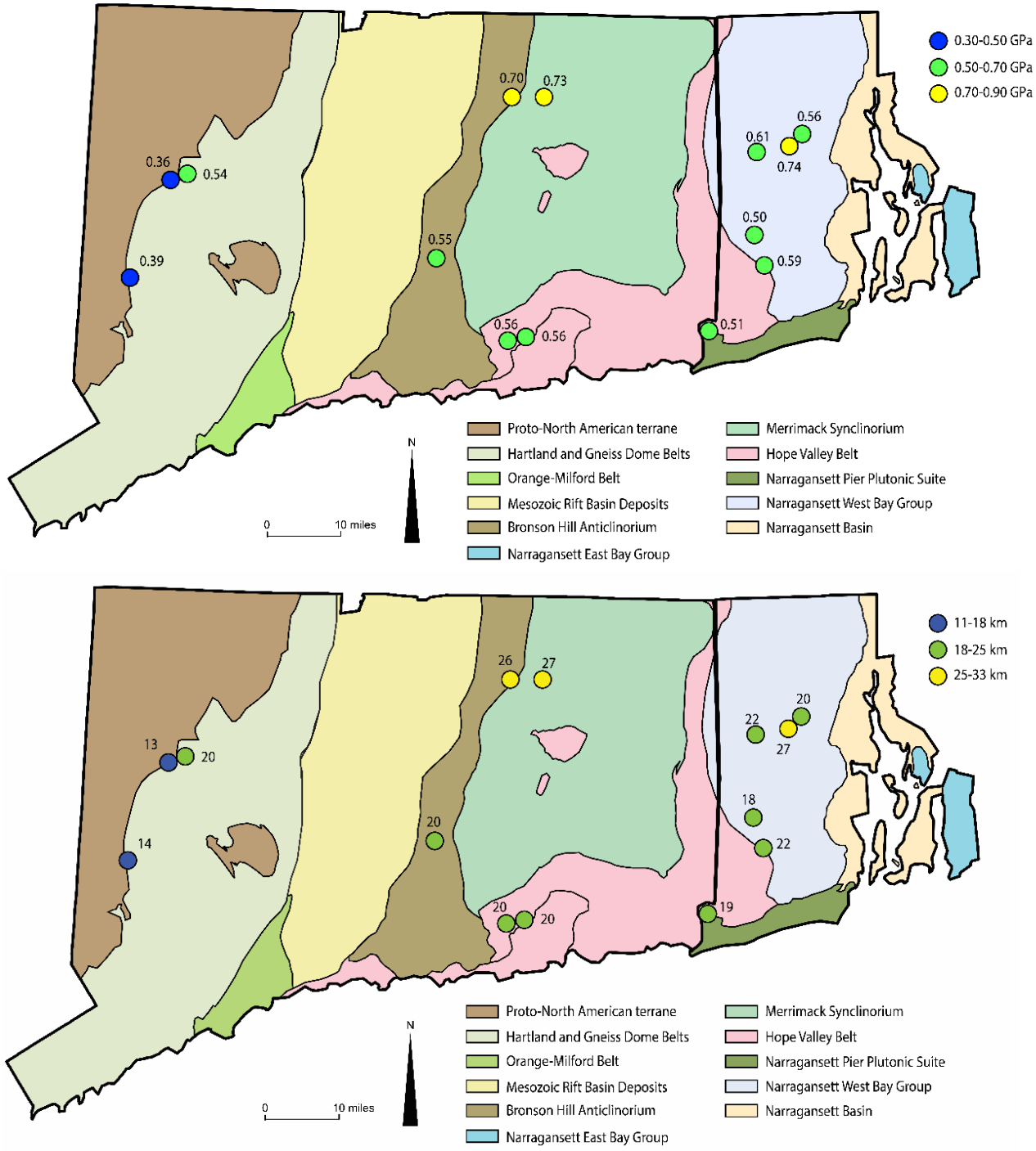

Figure 3. AH barometer pressure (top) and depth (bottom) estimates from this study calculated with the calibration of Ague (1997). Depth estimated as in Figure 2.

Anderson (1996) calculated pressures of plutons in the Mojave Desert and found at least two discrete depth clusters: a shallow set centered at ~0.2 GPa and a deeper set centered at ~0.6 GPa.

The lowest pressures are from samples NE11 (discussed above) and NE131, which are both from the Brookfield plutonic series immediately east of Cameron's Line. Sevigny and Hanson (1995) provided an age estimate of 454 ± 3 Ma for the unit and proposed that the Brookfield plutonic series could be part of the roots of a magmatic arc that cross-cuts Taconian deformation. The series has since been related to the initiation of west-dipping subduction following subduction polarity reversal (Moench and Aleinikoff, 2003) (Chu et al. 2016).

Higher pressures of ~0.7 GPa are recorded proximal to each other in northeastern Connecticut in the northern Bronson Hill Anticlinorium (BHA) and southern Central Maine Terrane (CMT). Hollocher et al. (2002) interpret the Monson Hill gneiss (from which the BHA sample is taken) to be part of a composite batholithic terrane underlying the Taconic arc that formed during its collision with the Laurentian margin. Ages of 454-442 ± 3 Ma for the Monson Hill gneiss suggest that it was emplaced during a period when the eastward dipping slab was rolling back or detaching, causing mantle upwelling, additional mantle and crustal melting and possibly a westward migration in the magmatic axis. The origin of the felsic igneous bodies of the southern CMT is not well understood, but the Brimfield schist from which the sample is taken has been shown to have reached pressures of at least 1.8 GPa and is home to the only identified UHT (>1000°C) metamorphic rocks in the United States (Ague and Eckert 2012). The presence of UHT, high pressure metamorphic rocks and deeply-emplaced igneous rocks demonstrate the deep exhumation that has occurred in north-central Connecticut.

Metamorphic pressure estimates (Figure 2) are generally higher than the calculated igneous pressures of crystallization for Connecticut and Rhode Island (Figure 3). This is compatible with situations in which A) plutons are emplaced prior to peak metamorphism and are subsequently buried deeper but retain their primary Al-in-hornblende signal and B) plutons

are emplaced following peak metamorphism at a shallower depth, while the surrounding metamorphic rocks retain their peak metamorphic pressure signal. It is likely that both of these processes account for the overall trend. Geobarometric and chronological studies of the metamorphic rocks immediately surrounding plutonic rocks are necessary to distinguish between these possibilities at any given locality.

In a detailed study of the Lyme Dome, Walsh et al. (2007) modeled a loading and exhumation history for coastal Connecticut based on regional geochronology and local thermochronology. The model predicts a burial and exhumation path associated with the Alleghanian orogeny. For rocks now at the surface, the path begins in the Carboniferous at a pressure of ~0.4 GPa, rises to a pressure of ~1.2 GPa that lasts from ~310-280 Ma, and then is exhumed to less than 0.5 GPa by 250 Ma (Figure 14, Walsh et al. 2007). The peak metamorphic temperature is estimated to be ~775°C. The rocks from the Lyme Dome sampled for barometry in this study (Lyme 1A-2, Lyme 1C-2, and Lyme 6A-2) are of Neoproterozoic age and give consistent crystallization pressure estimates of 0.56 GPa. These estimates provide another point on the P-T-t paths modeled by Walsh et al., albeit several hundred million years prior to the beginning of the Alleghanian orogeny. The P-T-t paths, geobarometric measurements, and homogeneous BSE appearance of the hornblendes together support the assertion that aluminum in hornblende is not likely to reset during metamorphism after crystallization, even when metamorphic pressures are more than double that of crystallization, temperatures approach or exceed 650°C, and peak metamorphic conditions are maintained for long periods (up to 30 Myr). Similar conclusions can be drawn from samples in the Bronson Hill Anticlinorium (NE38 and JAQ-246A-1), for which AH pressures are 0.55 and 0.70 GPa respectively. Wintsch et al. (2003) carried out similar loading and exhumation modeling for locations within the Bronson Hill

Anticlinorium (see Figure 7 in Wintsch et al.). For the locations nearest to NE38 and JAQ-246A-1, peak pressures were estimated to be 1.20 and 1.10 GPa, with peak metamorphic temperatures of ~510°C and 700°C respectively.

The Scituate Igneous Suite is the only body of igneous rock analyzed in this study for which a depth of crystallization has previously been ventured. Buddington classified the "Scituate Granite Gneiss" as mesozonal, corresponding to 0.20-0.45 GPa (Buddington 1959). Four pressure estimates were calculated for the Scituate Igneous Suite in this study (NE86, NE98, NE100 and NE107), for which pressures range from 0.50 GPa – 0.74 GPa. Although the high-pressure end of the mesozone falls slightly within the error of the lowest barometry pressure (0.50 GPa ± 0.06 GPa), the majority of the analyses are outside of Buddington's mesozone, suggesting that either 1) the mesozone is deeper than theorized by Buddington or 2) the Scituate Igneous Suite is instead catazonal.

4.1 Igneous Rock Classification

While the igneous thin sections were being searched for hornblende to be used for barometry, the presence or absence of muscovite and garnet was noted in order to broadly characterize the samples on a compositional basis. The distribution of these minerals, as well as that of hornblende, is shown in Figure 4. The presence of garnet and muscovite is taken to indicate that the rocks are peraluminous (Villaseca et al. 1998), meaning that the proportion of Al_2O_3 is larger than the combined proportion of CaO, Na_2O and K_2O (Shand 1927). Peraluminous rocks are primarily generated by the melting of a variety of crustal rocks, foremost among which are metasediments (metapelites), greywackes, orthogneisses and amphibolites. They are most abundant in intracontinental collisional orogens (Villaseca et al. 1998), though they are also important in magmatic arc settings. Rocks containing hornblende lacking in

muscovite are taken to be metaluminous (Frost et al. 2001)., meaning that the proportion of Al_2O_3 is smaller than the combined proportion of CaO, Na_2O and K_2O. As can be seen in Figure 4, the abundance of muscovite and garnet in Connecticut indicates the widespread distribution of peraluminous rocks, especially in the Taconic accretionary prism in the western half of the state. This suggests the considerable involvement of crustal material (of the types mentioned above) in the genesis of these rocks, likely as the primary source of the magma. The Rhode Island rocks observed are predominantly metaluminous, especially those of the Scituate Igneous Suite. The Scituate Igneous Suite is a complex assortment of igneous rocks that is theorized to be the result of crustal melting generated by a pulse of magmatism associated with late Devonian rifting (Thompson and Hermes 2003). The metaluminous character of these rocks suggests that the crustal material that melted to form them was metaigneous.

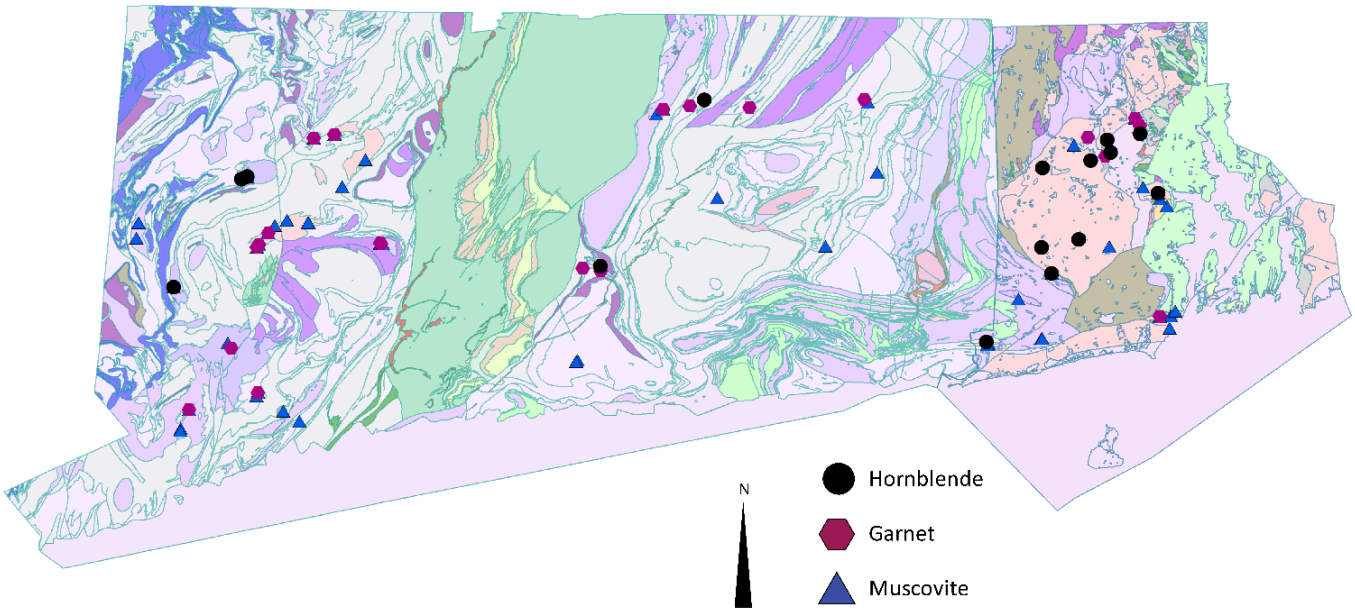

Figure 4. Map of the study area showing the distribution of hornblende, garnet and muscovite in the samples studied.

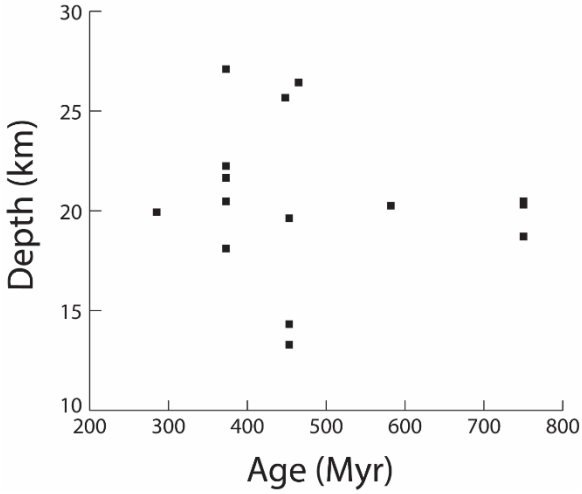

Figure 5. Graph of emplacement depth versus age.

No relationship was found between the age of intrusion and depth of emplacement (Figure 5). This is consistent with Buddington's assertion that there is no such relationship for rocks older than the Paleogene (Buddington 1959) and underscores the variability of exhumation rate throughout the region, as a spatially uniform exhumation rate would generate a positive relationship between intrusion age and depth of exposure.

TABLE 1. Sample Information

Sample	Latitude	Longitude	Intrusion	Age (Ma)	Pressure (Schmidt 1992)	Depth (Mutch et al. 2016)	Depth (Ague 1996)
NE10	41.71098	-73.2648	Brookfield Gneiss	453 ± 3	0.61	0.48	0.54
NE11 Bright BSE	41.716	-73.253	Brookfield Gneiss	453 ± 3	0.63	0.49	0.55
NE11 Med. BSE	41.716	-73.253	Brookfield Gneiss	453 ± 3	0.38	0.30	0.36
NE11 Dark BSE	41.716	-73.253	Brookfield Gneiss	453 ± 3	0.35	0.28	0.34
NE131 Bright BSE	41.50015	-73.3971	Brookfield Gneiss	453 ± 3	0.42	0.33	0.39
NE131 Med. BSE	41.50015	-73.3971	Brookfield Gneiss	453 ± 3	0.03	0.12	0.12
NE38	41.54151	-72.5644	Maromas Granite Gneiss	285 ± 10	0.62	0.49	0.55
NE48	41.52698	-71.6838	Scituate Igneous Suite	373 ± 7	0.68	0.54	0.59

NE57	41.39343	-71.8111	Mamacoke Formation	> Late Proterozoic	0.58	0.45	0.51
NE86	41.57764	-71.7035	Scituate Igneous Suite	373 ± 7	0.55	0.43	0.50
NE98	41.73291	-71.7015	Scituate Igneous Suite	373 ± 7	0.70	0.56	0.61
NE100	41.74752	-71.6082	Scituate Igneous Suite	373 ± 7	0.87	0.73	0.74
NE103	41.79962	-71.5112	Scituate Igneous Suite alkali feldspar granite	373 ± 7	-	-	-
NE107	41.78783	-71.5755	Scituate Igneous Suite	373 ± 7	0.64	0.50	0.56
JAQ246A-1	41.86607	-72.3615	Monson Gneiss	442-454 +3/-2	0.82	0.68	0.70
JAQ365A	41.87085	-72.2738	Igneous member of Brimfield Schist	Ordovician	0.85	0.71	0.73
Lyme 1A-2	41.36547	-72.3693	Rope Ferry Gneiss	Neoproterozoic	0.64	0.50	0.56
Lyme 1C-2	41.36547	-72.3693	Rope Ferry Gneiss	Neoproterozoic	0.63	0.50	0.56
Lyme 6A-2	41.37007	-72.3244	Lord Hill gneiss	582 ± 9	0.63	0.50	0.56

5. Pseudosection Results

Pseudosections were generated for a variety of compositions using older and newer thermodynamic data and theriak-domino software. Compositions and databases used to produce pseudosections are shown in Table 2. All pseudosections in Table 2 were considered in generating the bathograd scheme of Figure 7, but only selected pseudosections will be shown to demonstrate certain points.

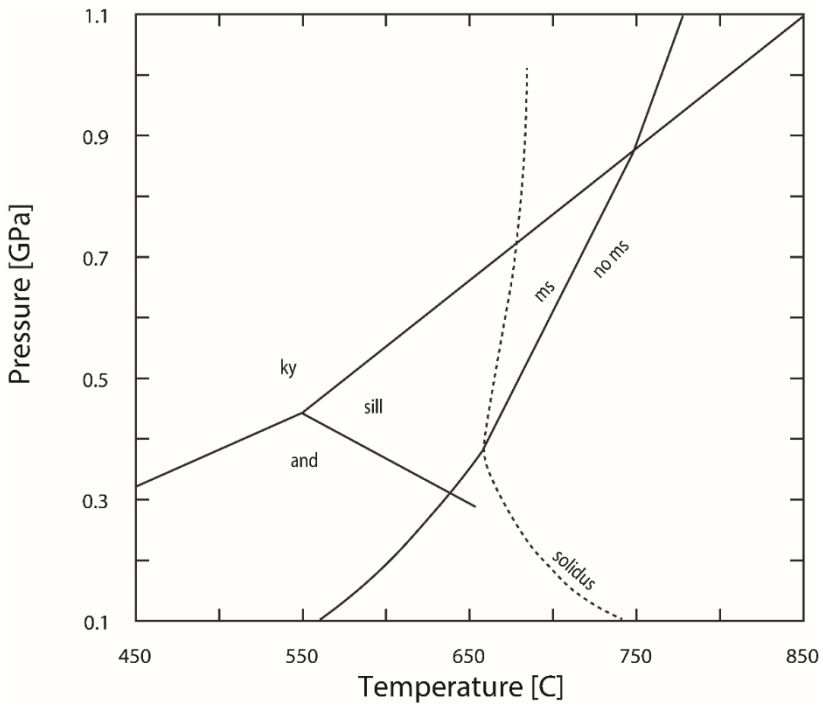

Figure 6. Simplified version of pseudosection 3a showing key phases (see Table 2 for composition and database used). Note the complete absence of staurolite. ky=kyanite, sill=sillimanite, and=andalusite, ms=muscovite.

TABLE 2. Pseudosection Compositions

Pseudosection	Bulk Composition	Fe ratio	H_2O	Database
1a	A91	W14	Saturated	old
1b	A91	W14	Saturated	new
2a	A91	W14	Saturated	old
2b	A91	W14	Undersaturated	new
3a	A91	A91	Undersaturated	old
3b	A91	A91	Saturated	new
4	A91	A91	Saturated	new
5a	JAW-21	JAW-21	Saturated	old
5b	JAW-21	JAW-21	Saturated	new

Note: A91 refers to the average amphibolite facies composition of Ague (1991). W14 refers to the Fe ratio employed by White et al. (2014). Psuedosection 2b is Figure 8 from White et al. (2014). The "old" database is from 3.01.2012 while the "new" database is from 4.02.2017.

Most significantly influenced by the database used is the staurolite stability field. Strikingly, the new database produces large staurolite stability fields for all compositions used, while only one pseudosection using the old database has significant staurolite. This contrast can be seen in Figures 6 and 7, which use the water-undersaturated amphibolite composition of Ague (1991) and the old and new database respectively. White et al. (2014) generated pseudosections using the new database and the composition of Ague (1991), but with a higher Fe^{3+} / Fe^{2+}. This more oxidized composition would be expected to produce a large staurolite stability field, as the formation of abundant oxide phases stifles garnet and biotite formation, in turn leaving more aluminum for aluminous phases like staurolite. Their pseudosection exhibits the expected large staurolite stability field (Figure 9), but a pseudosection generated in this study with the same composition using the old database has negligible staurolite (Figure 8). These drastic changes in staurolite stability raise concerns over the mineral's value as a predictor of P-T conditions.

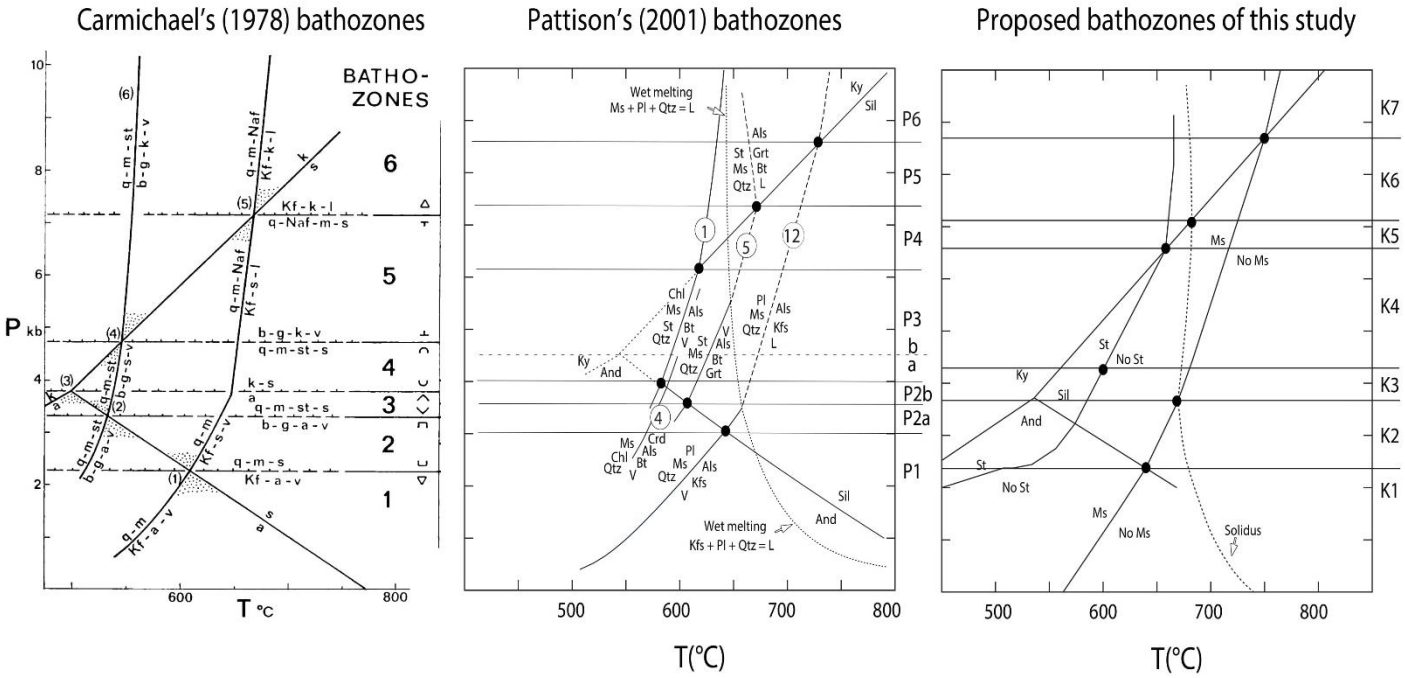

Figure 7. A comparison of bathograd schemes from this study and previous studies. The pseudosection shown for this study is 3b and is representative of the average bathograd positions for all pseudosections generated. Mineral abbreviations are described in Figure 6 caption, with the addition of St=staurolite.

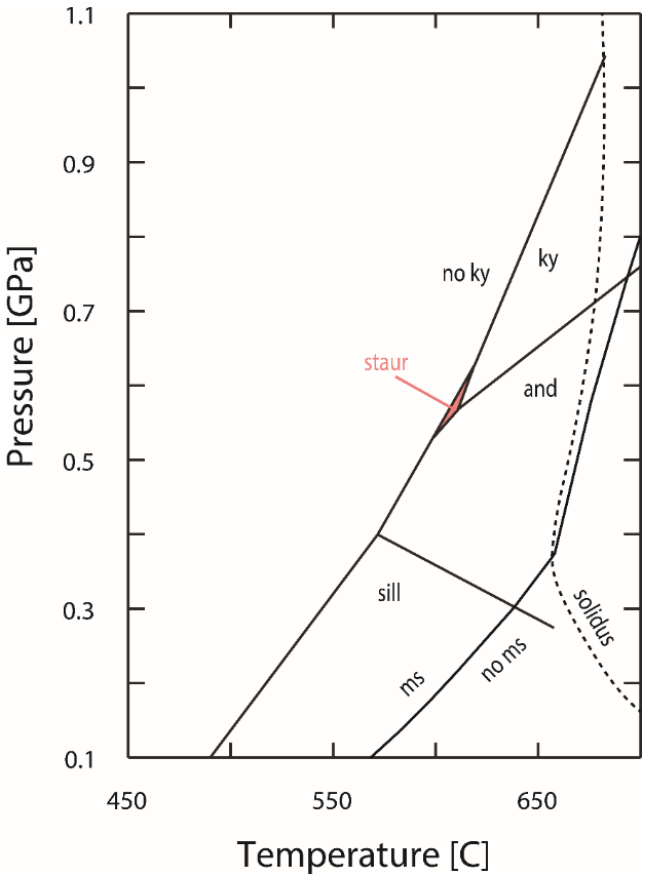

Figure 8. Simplified version of pseudosection 2a showing key phases. Note the very small staurolite field compared to that of Figure 9, which uses the same exact composition but a newer database.

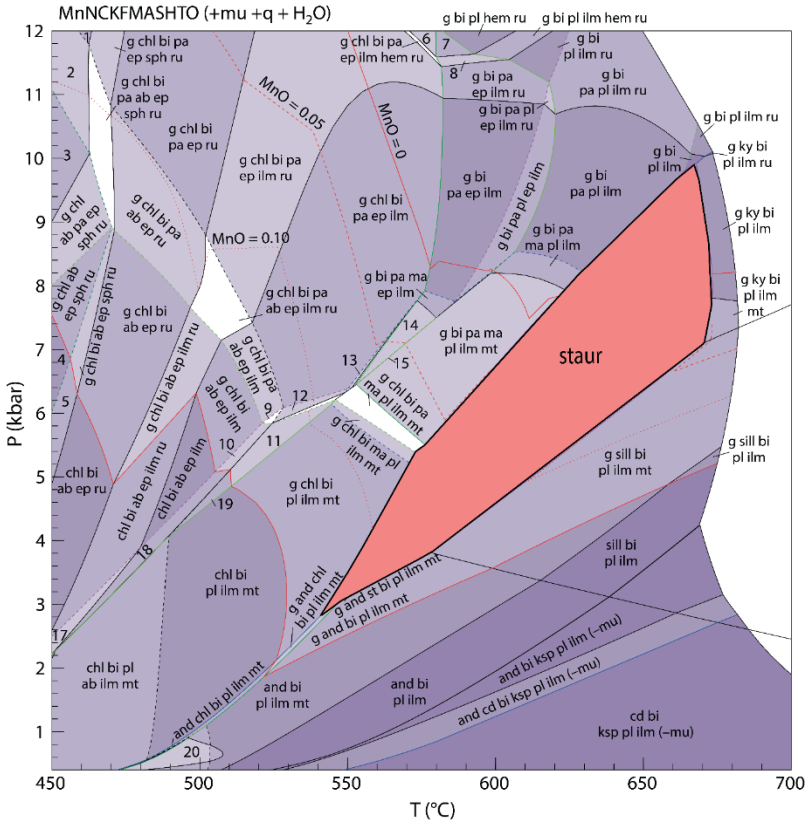

Figure 9. Pseudosection 2b (modified from White et al. 2014, Figure 8), with the staurolite field highlighted.

5.1 Pseudosection Bathograds

Bathograds, as first described by Carmichael (1978), can be drawn where two reaction lines intersect such that two mineral assemblage stability fields meet at an invariant point but do not overlap in pressure. Bathograds that do not vary significantly in position due to changes in bulk composition or the dataset used to calculate them are the most reliable for P-T estimates. Among the nine pseudosections generated using different compositions and datasets, six bathograds were identified that were present in most pseudosections and exhibited fairly consistent pressures. These bathograds are present in more or less their average positions in the pseudosection shown in Figure 7, where they are compared to the bathograd schemes of Carmichael (1978) and Pattison (2001). For the pressures at which bathograds are found in each pseudosection, see Table 3.

A discussion of the differences between the bathograd scheme proposed in this study and those of Carmichael and Pattison is in order. The bathograds of Carmichael and Pattison that rely on the general reaction quartz + muscovite + staurolite → garnet + biotite + aluminosilicate + vapor (Pattison reaction 5) are used but in a modified sense. This reaction's intersection with the kyanite-sillimanite line is present in all pseudosections bearing staurolite and is consistently at ~0.63 GPa and is therefore judged to be useful, while this reaction's intersection with the andalusite-sillimanite line is only present in one pseudosection and is excluded. Pattison's reaction 1 is not observed in any of this study's pseudosections so no bathograds are based on it. Also excluded is Carmichael's bathograd based on the aluminosilicate triple point because in the majority of metapelitic rocks, aluminosilicates do not develop until the rock has been heated to temperatures substantially above the triple point (Pattison, 2001). Bathograd KA3-KA4 is also unique to this study; it represents the minimum pressure at which staurolite is present in a rock

with a representative metamorphic temperature of 600°C. Neither Carmichael nor Pattison utilized the intersection of reactions with the solidus, but as melt is a phase that can be readily discerned in the field, bathograds utilizing the solidus could potentially be of use. Two bathograds are added using the solidus: one at the intersection of the muscovite stability line with the solidus and one at the intersection of the kyanite-sillimanite line with the solidus.

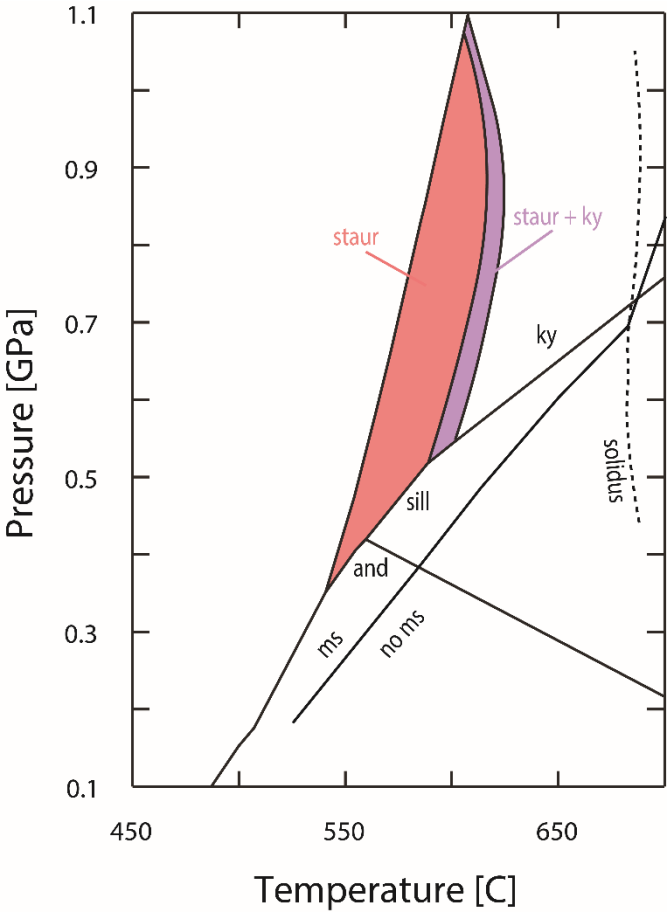

Figure 10. Simplified version of pseudosection 5a (metapelite composition from Wepawaug Schist) showing key phases.

A pseudosection worth noting is that of JAW-21 (Figure 10), which utilizes the composition of a representative metapelite of the Wepawaug Schist from Ague (2002). The higher aluminum content of this starting composition is likely the cause of the large staurolite stability field, which is present even in the pseudosection that uses the old database. Of note is the up-pressure displacement of the muscovite stability line relative to other pseudosections which causes its intersection with the solidus (KA2-KA3) to occur at a significantly higher pressure (0.7 instead of ~0.45 GPa). The adjusted position of this pseudosection's bathograds should be used for rocks that are particularly high in aluminum like JAW-21.

TABLE 3. Bathograd pressures for all pseudosections

	Other Studies		This Study									
Bathograd	Pattison	Carmichael	1a	1b	2a	2b	3a	3b	4	5a	5b	Average
KA1-KA2	0.3	0.22	0.3	0.31	0.31	0.31	0.31	0.31	0.31	0.39	0.35	0.32
KA2-KA3	0.35	-	0.38	0.42	0.38	0.42	0.37	0.42	0.42	0.7	0.57	0.45
KA3-KA4	0.33	-	-	0.46	-	0.48	-	0.48	0.48	0.55	0.47	0.49
KA4-KA5	0.63	0.47	-	0.7	-	0.7	-	0.69	0.69	0.55	0.7	0.67
KA5-KA6	0.68	-	0.72	0.74	0.72	0.74	0.72	0.73	0.74	0.73	0.74	0.73
KA6-KA7	0.85	0.72	0.75	-	0.77	-	0.86	0.88	0.78	0.77	-	0.80

Note: Where reaction intersections upon which a bathograd is based are not present in the pseudosection, a "-" is marked.

6. Summary

Plutonic emplacement pressures for the observed igneous rocks range from 0.34 GPa to 0.74 ± 0.06 GPa. Pressures are lowest immediately to the east of Cameron's Line in the Brookfield Plutonic Series, a part of the Taconic accretionary prism, while deeper pressures exceeding 0.70 GPa are found in the northern Bronson Hill Anticlinorium, the adjacent southern portion of the Central Maine Terrane, and at one location in the Avalonian Scituate Igneous Suite. The rocks of Avalonian affinity otherwise show little variation, falling between 0.5 and 0.61 GPa. More extensive barometric measurement of southern New England's plutonic rocks will be necessary to illustrate both local and regional patterns in emplacement pressure that are hinted at by this preliminary investigation. In addition, a survey of metamorphic mineral assemblages should be interpreted with the new set of bathograds proposed here, with the goal of

producing a bathozone map like that of Carmichael (1978) but based on more consistent bathograds and benefitting from a higher sample density.

7. Acknowledgements

This senior thesis would not have been possible without the work and guidance of Jay Ague, the technical assistance of Jim Eckert, the feedback of Dave Evans, nor the advice of Dave Auerbach and Mary-Louise Timmermans. Funding from the Karen L. Von Damm ‘77 Undergraduate Research Fellowships in Geology & Geophysics is gratefully acknowledged.

8. References Cited

Ague, J.J., 1991, Evidence for major mass transfer and volume strain during regional metamorphism of pelites: Geology, v. 19, p. 855-858.

Ague, J.J., 1997, Thermodynamic Calculation of Emplacement Pressures for Batholithic Rocks, California: Implications for the Aluminum-in-Hornblende Barometer: Geology, v. 25, p. 563-566.

Ague, J.J., 2002, Gradients in Fluid Composition across Metacarbonate Layers of the Wepawaug Schist, Connecticut, USA: Contributions to Mineralogy and Petrology, v. 143, p. 38–55.

Ague, J.J. and Brandon, M.T., 1996, Regional tilt of the Mount Stuart batholith, Washington, determined using aluminum-in-hornblende barometry: Implications for northward translation of Baja British Columbia: Geological Society of America Bulletin, v. 108, p. 471-488.

Ague, J.J. and Eckert Jr, J.O., 2012, Precipitation of rutile and ilmenite needles in garnet: Implications for extreme metamorphic conditions in the Acadian Orogen, USA: American Mineralogist, v. 97, p. 840-855.

Ague, J.J., Eckert Jr, J.O., Chu, X., Baxter, E.F. and Chamberlain, C.P., 2013, Discovery of ultrahigh-temperature metamorphism in the Acadian orogen, Connecticut, USA: Geology, v. 41, p.271-274.

Anderson, J.L., 1996, Status of thermobarometry in granitic batholiths: Earth and Environmental Science Transactions of The Royal Society of Edinburgh, v. 87, p. 125-138.

Anderson, J. L., Barth, A.P., Wooden, J.L., and Mazdab, F., 2008, Thermometers and Thermobarometers in Granitic Systems: Reviews in Mineralogy and Geochemistry, v. 69, p. 121–142.

Buddington, A. F., 1959, Granite Emplacement With Special Reference To North America: Geological Society of America Bulletin, v. 70, p. 671.

Carmichael, D. M., 1978, Metamorphic Bathozones and Bathograds; a Measure of the Depth of Post-Metamorphic Uplift and Erosion on the Regional Scale: American Journal of Science, v. 278, p. 769–797.

Chu, X., Ague, J.J., Axler, J.A., and Tian, M., 2016, Taconian Retrograde Eclogite from Northwest Connecticut, USA, and Its Petrotectonic Implications: Lithos, v. 240-243, p. 276–294.

Dietsch, C, 1989, The Waterbury Dome, West-Central Connecticut; a Triple Window Exposing Deeply Deformed, Multiple Tectonic Units: American Journal of Science, v. 289, p. 1070–1097.

Dipple, G. M., Wintsch, R.P., and Andrews, M.S., 1990, Identification of the Scales of Differential Element Mobility in a Ductile Fault Zone: Journal of Metamorphic Geology, v. 8, p. 645–661.

Frost, B.R., Barnes, C.G., Collins, W.J., Arculus, R.J., Ellis, D.J. and Frost, C.D., 2001, A geochemical classification for granitic rocks: Journal of petrology, v. 42, p. 2033-2048.

Grew, E.S. and Day, H.W., 1972, Staurolite, kyanite, and sillimanite from the Narragansett basin of Rhode Island: United States Geological Survey Professional Paper 800-D, p. D151–D157.

Hames, W.E., Tracy, R.J., and Bodnar, R.J., 1989, Postmetamorphic Unroofing History Deduced from Petrology, Fluid Inclusions, Thermochronometry, and Thermal Modeling: An Example from Southwestern New England: Geology, v. 17, p. 727.

Hames, W. E., Tracy, R.J., Ratcliffe, N.M., and Sutter, J.F., 1991, Petrologic, Structural, and Geochronologic Characteristics of the Acadian Metamorphic Overprint on the Taconide Zone in Part of Southwestern New England: American Journal of Science, v. 291, p. 887–913.

Hammarstrom, J.M. and Zen, E.A., 1986: Aluminum in hornblende: an empirical igneous geobarometer: American Mineralogist, v. 71, p. 1297-1313.

Hollocher, K., Bull, J. and Robinson, P., 2002, Geochemistry of the metamorphosed Ordovician Taconian magmatic arc, Bronson Hill anticlinorium, western New England: Physics and Chemistry of the Earth, Parts A/B/C, v. 27, p. 5-45.

Keller, D.S. and Ague, J.J., 2016, Silica-undersaturated garnet + spinel + corundum mineral assemblages record UHT metamorphism, Central Maine Terrane, Connecticut, USA: Geological Society of America Abstracts with Programs, p. 139-7.

Mader, U.K., and Berman, R.G., 1992: Amphibole thermobarometry, a thermodynamic approach: Current Research, Part E, Geological Survey of Canada, p.393-400.

Mäder, U. K., Percival, J. A., and Berman, R. G., 1994, Thermobarometry of garnetclinopyroxene-hornblende granulites from the Kapuskasing structural zone: Canadian Journal of Earth Sciences, v. 31, p. 1134–1145.

Moench, R.H. and Aleinikoff, J.N., 2002, Stratigraphy, geochronology, and accretionary terrane settings of two Bronson Hill arc sequences, northern New England: Physics and Chemistry of the Earth, Parts A/B/C, v. 27, p. 47-95.

Mutch, E.J.F., Blundy, J.D., Tattitch, B.C., Cooper, F.J. and Brooker, R.A., 2016, An experimental study of amphibole stability in low-pressure granitic magmas and a revised Al-in-hornblende geobarometer: Contributions to Mineralogy and Petrology, v. 171, p. 85.

Pattison, David R.M., 2001, Instability of Al2SiO5 ‘Triple-Point’ Assemblages in Muscovite+Biotite+Quartz-Bearing Metapelites, with Implications: American Mineralogist, vol. 86, p. 1414–1422.

Schmidt, M.W., 1992, Amphibole composition in tonalite as a function of pressure: an experimental calibration of the Al-in-hornblende barometer: Contributions to mineralogy and petrology, v. 110, p. 304-310.

Sevigny, J.H. and Hanson, G.N., 1995, Late-Taconian and pre-Acadian history of the New England Appalachians of southwestern Connecticut, Geological Society of America Bulletin, v. 107, pp. 487-498.

Shand, S.J., 1927, On the relations between silica, alumina, and the bases in eruptive rocks, considered as a means of classification: Geological Magazine, v. 64, p. 446-449.

Thompson Jr, J.B. and Norton, S.A., 1968, Paleozoic regional metamorphism in New England and adjacent areas: Studies of Appalachian geology: Northern and maritime, p. 319-327.

Thompson, M.D. and Hermes, O.D., 2003, Early rifting in the Narragansett Basin, Massachusetts–Rhode Island: evidence from Late Devonian bimodal volcanic rocks: The Journal of Geology, v. 111, p. 597-604.

Villaseca, C., Barbero, L. and Herreros, V., 1998, A re-examination of the typology of peraluminous granite types in intracontinental orogenic belts: Earth and Environmental Science Transactions of The Royal Society of Edinburgh, v. 89, p. 113-119.

Walsh, G. J., Aleinikoff, J.N., and Wintsch, R.P., 2007, Origin of the Lyme Dome and Implications for the Timing of Multiple Alleghanian Deformational and Intrusive Events in Southern Connecticut: American Journal of Science, vol. 307, p. 168–215.

White, R. W., Powell, R., and Johnson, T.E., 2014, The Effect of Mn on Mineral Stability in Metapelites Revisited: Newa-Xrelations for Manganese-Bearing Minerals: Journal of Metamorphic Geology, vol. 32, p. 809–828.

Wintsch, R. P., 2003, P-T-t Paths and Differential Alleghanian Loading and Uplift of the Bronson Hill Terrane, South Central New England: American Journal of Science, vol. 303, p. 410–446.

Zen, E., 1989, Plumbing the Depths of Batholiths: American Journal of Science, vol. 289, p. 1137–1157.

Appendix

TABLE 4. Hornblende analyses in weight percent

	NE10	NE11 Bright BSE	NE11 Med. BSE	NE11 Dark BSE	NE38	NE48	NE57	NE86	NE98	NE100
SiO2	42.10	44.00	46.90	47.90	41.60	40.70	43.55	38.74	38.34	37.49
TiO2	1.50	0.66	0.56	0.47	0.80	1.11	0.86	1.08	0.93	0.36
Al2O3	10.60	11.20	8.24	7.96	10.60	11.41	10.46	9.40	11.11	13.05
FeO(total)	16.80	13.80	12.00	11.00	24.50	21.45	15.97	31.40	31.58	31.03
Fe2O3	1.94	2.44	2.55	2.02	3.87	5.26	4.06	5.59	5.20	6.52
FeO	15.05	11.61	9.71	9.18	21.02	16.71	12.32	26.37	26.91	25.17
MnO	0.30	0.20	0.20	0.20	0.90	1.11	0.36	0.94	0.77	0.70
MgO	10.20	12.40	14.50	14.80	5.56	7.59	11.46	2.01	1.40	1.37
CaO	11.70	12.20	12.40	12.30	11.20	11.28	11.85	10.29	10.61	10.65
Na2O	1.40	1.30	1.00	1.00	1.30	1.47	1.23	1.79	1.49	1.38
K2O	1.60	1.30	0.78	0.74	1.30	1.55	1.24	1.62	2.03	2.05

F	0.20	0.20	0.10	0.20	0.10	0.30	1.46	0.38	0.31	0.28
Cl	0.13	0.11	0.10	0.04	0.02	0.02	0.08	0.15	0.12	0.12
Total	96.53	97.37	96.78	96.61	97.88	97.98	98.52	97.79	98.69	98.49
Total*	96.61	97.51	96.97	96.72	98.22	98.38	98.29	98.16	99.06	99.00

	NE103 Bright BSE	NE103 Med. BSE	NE107	NE131 Bright BSE	NE131 Med. BSE	JAQ 246A-1	JAQ 365A	Lyme 1A-2	Lyme 1C-2	Lyme 6A-2
SiO2	51.18	52.01	38.50	48.40	53.80	39.90	39.73	41.74	41.88	41.91
TiO2	0.08	0.13	0.39	0.58	0.17	0.83	0.87	1.54	1.53	1.76
Al2O3	0.95	1.29	10.32	8.90	4.19	13.00	13.38	11.04	10.99	10.96
FeO(total)	37.69	29.66	34.18	11.00	8.50	21.50	22.31	19.98	20.20	19.56
Fe2O3	7.65	8.76	6.02	1.87	1.35	6.10	5.29	3.97	3.94	3.28
FeO	30.81	21.78	28.77	9.31	7.29	16.01	17.56	16.41	16.66	16.61
MnO	0.42	0.35	0.87	0.35	0.32	0.79	0.62	0.83	0.63	0.63
MgO	0.09	0.04	0.31	14.80	17.80	7.21	6.71	8.56	8.63	8.87
CaO	0.41	5.51	10.14	12.20	12.50	11.20	11.31	11.36	11.38	11.35
Na2O	6.28	9.89	1.49	0.93	0.45	1.20	1.34	1.39	1.42	1.47
K2O	0.24	0.01	2.29	0.63	0.17	1.70	1.86	0.83	1.53	1.55
F	0.01	0.01	0.15	0.00	0.00	0.00	0.09	0.27	0.26	0.17
Cl	0.00	0.00	0.03	0.00	0.00	0.10	0.34	0.07	0.06	0.26
Total	97.37	98.91	98.66	97.79	97.90	97.43	98.55	97.61	98.51	98.51
Total*	98.13	99.78	99.19	97.98	98.03	98.02	98.97	97.88	98.78	98.70

*Note: Total*Incorporates estimated FeO and Fe2O3 weight percents and subtracts oxygen equivalent of F and Cl*

TABLE 5. Hornblende analyses based on 23 O

	NE10	NE11 Bright BSE	NE11 Med. BSE	NE11 Dark BSE	NE38	NE48	NE57	NE86	NE98	NE100
Si	6.433	6.536	6.892	6.979	6.450	6.245	6.512	6.290	6.170	6.000
Ti	0.173	0.073	0.062	0.052	0.093	0.129	0.096	0.131	0.113	0.044
Al IV	1.567	1.464	1.108	1.021	1.550	1.755	1.488	1.710	1.831	2.000
Al VI	0.346	0.490	0.320	0.346	0.384	0.308	0.356	0.088	0.277	0.463
Al_{tot}	1.912	1.954	1.428	1.368	1.935	2.064	1.843	1.798	2.107	2.462
Fe3+	0.224	0.271	0.274	0.230	0.452	0.607	0.457	0.683	0.630	0.785
Fe2+	1.928	1.438	1.162	1.161	2.728	2.145	1.540	3.580	3.621	3.369
Mg	2.328	2.735	3.180	3.219	1.286	1.735	2.553	0.486	0.336	0.326
Mn	0.039	0.024	0.025	0.027	0.119	0.145	0.046	0.129	0.104	0.095

Ca	1.921	1.934	1.951	1.926	1.866	1.854	1.898	1.790	1.830	1.827
Na A site	0.042	0.035	0.026	0.039	0.071	0.078	0.054	0.112	0.091	0.092
Na B site	0.379	0.337	0.272	0.244	0.334	0.358	0.302	0.452	0.374	0.337
Na_{tot}	0.421	0.372	0.298	0.283	0.405	0.436	0.356	0.564	0.464	0.430
K	0.314	0.254	0.146	0.137	0.266	0.303	0.236	0.335	0.416	0.420
F	0.107	0.086	0.056	0.072	0.065	0.146	0.069	0.194	0.156	0.140
Cl	0.034	0.028	0.013	0.011	0.006	0.004	0.021	0.041	0.032	0.033
OH	1.859	1.886	1.931	1.917	1.929	1.849	1.910	1.765	1.812	1.827

	NE103 Bright BSE	NE103 Med. BSE	NE107	NE131 Bright BSE	NE131 Med. BSE	JAQ 246A-1	JAQ 365A	Lyme 1A-2	Lyme 1C-2	Lyme 6A-2
Si	8.077	7.950	6.252	6.958	7.560	6.113	6.085	6.337	6.345	6.351
Ti	0.009	0.015	0.048	0.063	0.018	0.096	0.100	0.176	0.175	0.200
Al IV	0.000	0.050	1.749	1.042	0.441	1.887	1.915	1.663	1.655	1.649
Al VI	0.177	0.183	0.227	0.466	0.253	0.471	0.499	0.313	0.308	0.309
Al_{tot}	0.177	0.233	1.975	1.508	0.694	2.358	2.414	1.976	1.963	1.959
Fe3+	0.908	1.007	0.736	0.201	0.143	0.704	0.609	0.453	0.449	0.374
Fe2+	4.067	2.785	3.907	1.110	0.858	2.052	2.249	2.084	2.111	2.105
Mg	0.021	0.009	0.075	3.172	3.730	1.648	1.531	1.937	1.948	2.004
Mn	0.056	0.046	0.119	0.043	0.039	0.103	0.080	0.107	0.081	0.081
Ca	0.070	0.903	1.764	1.882	1.887	1.843	1.856	1.849	1.848	1.844
Na A site	1.692	2.052	0.126	0.063	0.072	0.084	0.077	0.081	0.081	0.083
Na B site	0.231	0.879	0.343	0.198	0.051	0.279	0.322	0.328	0.335	0.350
Na_{tot}	1.923	2.931	0.468	0.261	0.123	0.363	0.399	0.408	0.416	0.433
K	0.049	0.002	0.474	0.115	0.031	0.325	0.362	0.297	0.295	0.300
F	0.003	0.007	0.080	0.042	0.035	0.023	0.044	0.127	0.123	0.083
Cl	0.001	0.001	0.008	0.001	0.001	0.019	0.088	0.018	0.017	0.067
OH	1.996	1.992	1.913	1.957	1.964	1.958	1.868	1.855	1.861	1.850